Table of contents

1. Materials

PMII ≥ 98%, ACS grade I_2 ≥ 99.8%, guanidinium thiocyanate (GuNCS) ≥ 97%, EDOT 97%, Alconox, Titanium(IV) isopropoxide ($Ti(OiPr)_4$), 4-tert-Butylpyridine (4-tBuPy) 96%, $SnCl_2$ 98% and solvents (anhydrous Acetonitrile (ACN) 99.8%, ACS grade 2-propanol ≥ 99.8%, ACS grade absolute Ethanol (EtOH), 99.9% 1-butanol) were purchased from Sigma-Aldrich and used as received.

Ultra dry LiI 99.999% and MgI_2 > 99% were bought from Fluka, $LiClO_4$ ≥ 99% was purchased from Acros organics.

FTO TEC-7 was bought from NSG, 18NR-T and 18NR-AO TiO_2 pastes were purchased from Greatcell Solar, the high stability electrolyte (HSE) was bought from Dyesol. Surlyn 25 was supplied from Dyepower Consortium.

N 719 was synthesized according to previous directions[1]. SnO_2 paste was prepared according to published procedures[2].

The FeNHC complex **C1** was prepared according to ref 3.[3]

2. Instruments and Methods

Absorption spectra of the photoanodes were collected with an agilent Cary 300 UV-Vis spectrophotometer at RT against a reference constituted by an undyed photoanode belonging to the same preparative batch.

The CVs were obtained with a PGSTAT 302N potentiostat in a three electrode cell using Pt as a counter electrode, a double jacketed SCE as a reference and the dyed TiO_2 thin film a working electrode in ACN/0.1 M $LiClO_4$.

Photo-electrochemical measurements were conducted with a PGSTAT 302N potentiostat coupled with an ABET technologies AM 1.5G sun simulator. The lamp irradiance was set to 100mW/cm^2.The J/V curves were carried out by cyclic voltammetry at scan rate of 20mV/s. Incident photon-to-current efficiency (IPCE) was measured under the monochromatic illumination generated by an air-cooled Luxtel 175 W Xe lamp coupled to an Applied Photophysics monochromator. Nova 1.11 controlled data acquisition during all electrochemical and photoelectrochemical measurements.

Transient absorption spectroscopy (TAS) was carried out on the sensitized thin films in contact with various electrolytes with an instrumental setup described elsewhere[4] using the 532 nm harmonic of

a nanosecond Nd:YAG laser (Continuum Surelite II) and a monochromatic probe beam. Various neutral filters were used to set the laser fluence at the desired value and appropriate input impedances, varying from 50 to 1 MOhm were used to amplify the transient signals on the appropriate time scales.

AFM images of the different electrodic substrates were collected with a Digital Instruments Nanoscope III scanning probe microscope (Digital Instruments, CA). The instrument was equipped with a silicon tip (RTESP-300 Bruker) and operated in tapping mode. Surface topographical analysis of raw AFM images was carried out with NanoScope analysis 1.5 program.

FT-IR were measured on a Bruker Vertex 70 FT-IR in diffuse reflectance mode by using either **C1** dispersed in KBr or loaded on Degussa P25 TiO_2 powder. In order to avoid saturation, the dyed P25 was disperded in KBr until obtaining a good S/N ratio without showing saturated bands. Frequency calculations were performed by DFT on the optimized structures of **C1** in fully protonated, anionic and coordinated to Ti(IV) forms. Optimization was carried in vacuo at the B3LYP/LANL2DZ level by using Gaussian 09 A 02.

3. Cell fabrication

FTO glasses were cleaned in Alconox solution and then with 2-propanol using an ultrasonic bath for 10' and then heated at 450°C for 20' to remove organic residuals. A blocking underlayer (*BUL*) was fabricated by spin-coating (10" at 1000 rpm followed by 20" at 2000 rpm) using a 0.3 M titanium tetraisopropoxide solution in 1-butanol followed by heating at 500 °C for 15". The TiO_2 colloidal paste (18NR-T and 18NR-AO) was cast by doctor blading. The resulting wet films were placed in an oven where semiconductor sintering occurred according to the following temperature program: 25−120 °C (10 min), 120−450 °C (30 min), 450 °C (20 min), 450−500 °C (10 min), 500 °C (10 min). Cooling at RT occurred naturally by stopping heating. $TiCl_4$ treatment was performed by drop casting a 0.4 M aqueous $TiCl_4$ solution on top of the semiconductor substrate followed by slow hydrolysis at room temperature in a closed chamber overnight. Later, after rinsing the substrates from the excess $TiCl_4$ solution with deionized water, a final annealing stage was carried out at 450 °C for 30'. The resulting thin films were stained by immersion in a 0.2 mM of acetonitrile solution of **C1** with 0.04 mM of chenodeoxycholic acid. Similar adsorption conditions were used for N 719 adsorption from ethanolic solution.

FTO substrates for the fabrication were first treated by spin coating a 0.3 M $SnCl_2$ in EtOH according to the same protocol described above. Following heating at 500 °C for 15 min the SnO_2 blocking

underlayer (*BUL*) was obtained. Mesoporous SnO_2 was obtained by blade casting an aqueous SnO_2 paste[2] on top of the compact SnO_2 layer, followed by sintering at 500 °C. A final treatment with $TiCl_4$ in order to improve the adsorption capability of these photoanodes was performed, as described above.

PEDOT counter electrodes were prepared by electropolymerization of EDOT on top of FTO by using a 10^{-2} M EDOT/0.1 M $LiClO_4$ acetonitrile solution in a three electrode cell using FTO as working electrode, a titanium foil as a cofacial counter electrode placed at ca. 3 mm distance from the working electrode and double jacket SCE as a reference electrode. The deposition was performed by scanning twice from 0 V to 1.7 V vs SCE at 50mV/s.[5]

Cells were prepared in an open configuration using surlyn 25 as a spacer. Redox electrolytes were prepared according to the following formulations, *electrolyte 1 (el1):* 0.1 M LI, 0.6 M PMII, 0.1 M I_2, 0.05 M MgI_2 in acetonitrile; *electrolyte 2(el2):* 0.1 M LI, 0.6 M PMII, 0.1 M I_2, 0.1 M MgI_2, 0.1 M GuNCS in Acetonitrile; *electrolyte 3 (el3)*: 0.1 M LI, 0.6 M PMII, 0.1 M I_2, 0.05 M MgI_2, 0.2 M 4-tBuPy in acetonitrile; commercial HSE (High stability electrolyte).

4. Diode equation

DSSCs have been showed to follow diode equation according to[6]

$$I = I_{photo} - I_0\left(\exp\left(-\frac{e(V+IR_s)}{nKT}\right) - 1\right) - \frac{V+IR_s}{R_{sh}}$$

Where I is the total current produced by the device at a given voltage Va. Iphoto is directly proportional to absorbed photon flux, I0 is the dark current which flows through the non-ideal diode (ideality factor n) at the applied forward voltage Va= (V+IRs) where Rs is the sum of the series resistance in the cell (given by contact resistance, charge transfer resistances and diffusional resistance). Va/Rsh accounts for charge leaks via short circuits in the cell, typically reaction of electrons with the redox couple at the ohmic contacts, and is most visible at low forward voltages, where the diode dark conductivity is low.

5. Spectroscopic and electrochemical measurements on semiconductor thin films

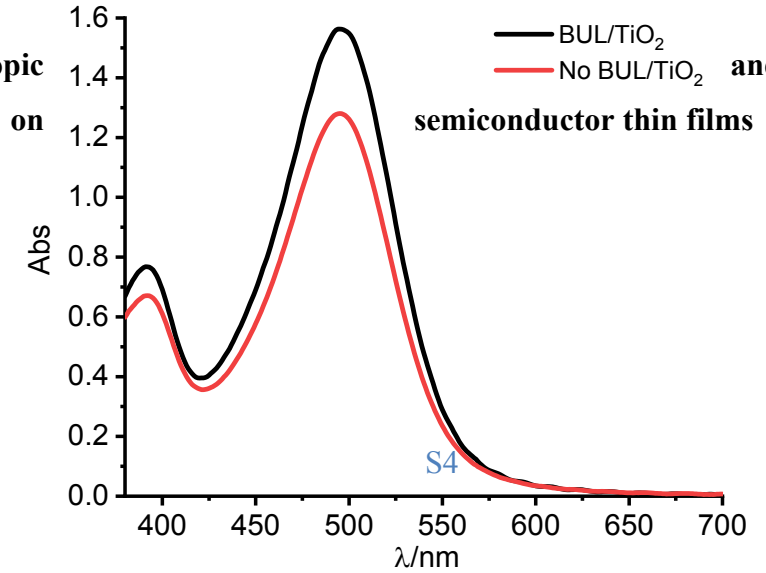

Figure S1: UV-Vis spectra of **C1** recorded on Transparent TiO_2 with (black) and without (red) blocking underlayer (*BUL*)

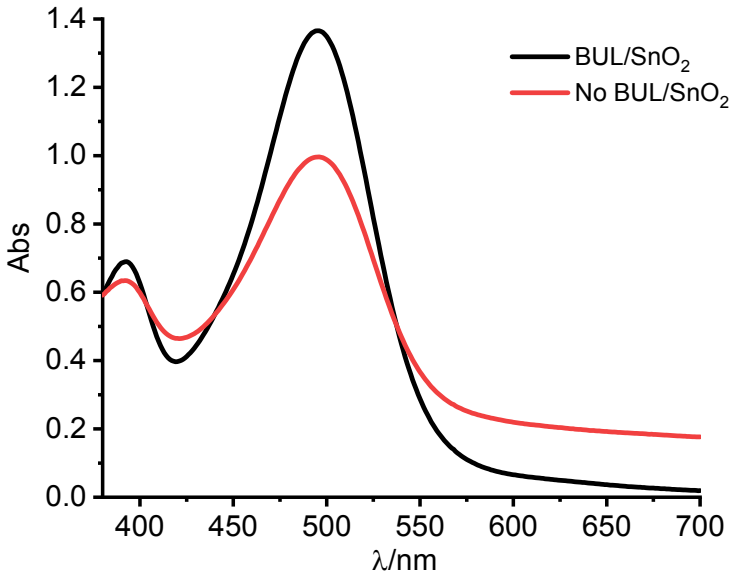

Figure S2: UV-Vis spectra of **C1**/SnO_2 recorded with (black) and without (red) blocking underlayer

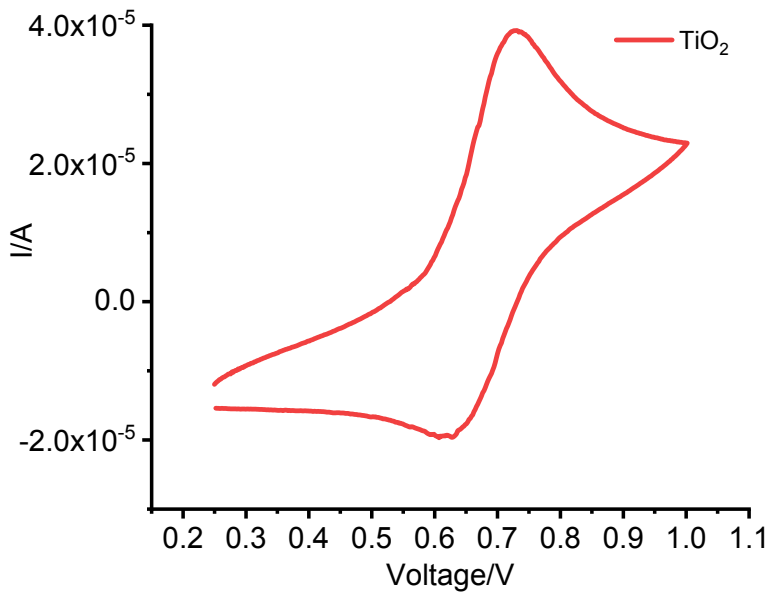

Figure S3: CV of **C1**/TiO_2 electrodes, 20 mV/s, referred to SCE. 0.1 M $LiClO_4$ in ACN

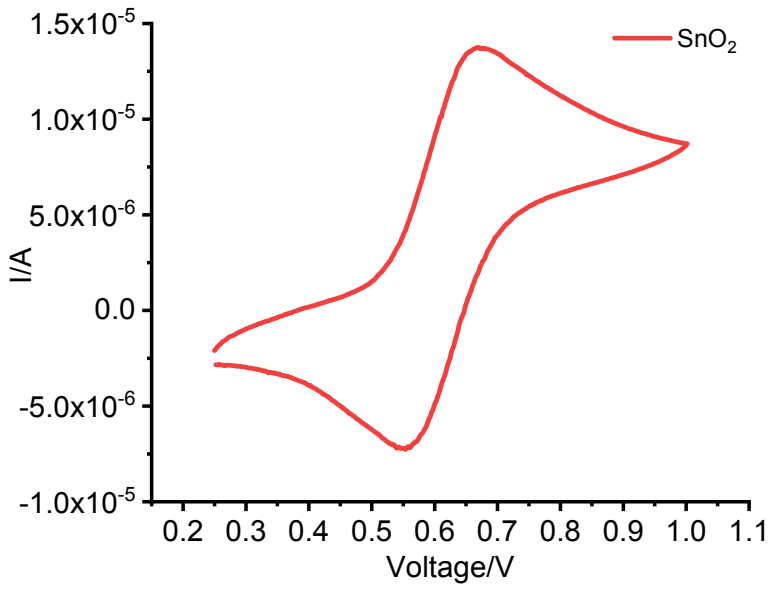

Figure S4: CV of **C1**/SnO_2 electrodes, 20 mV/s, referred to SCE. 0.1 M $LiClO_4$ in ACN

6. AFM characterization

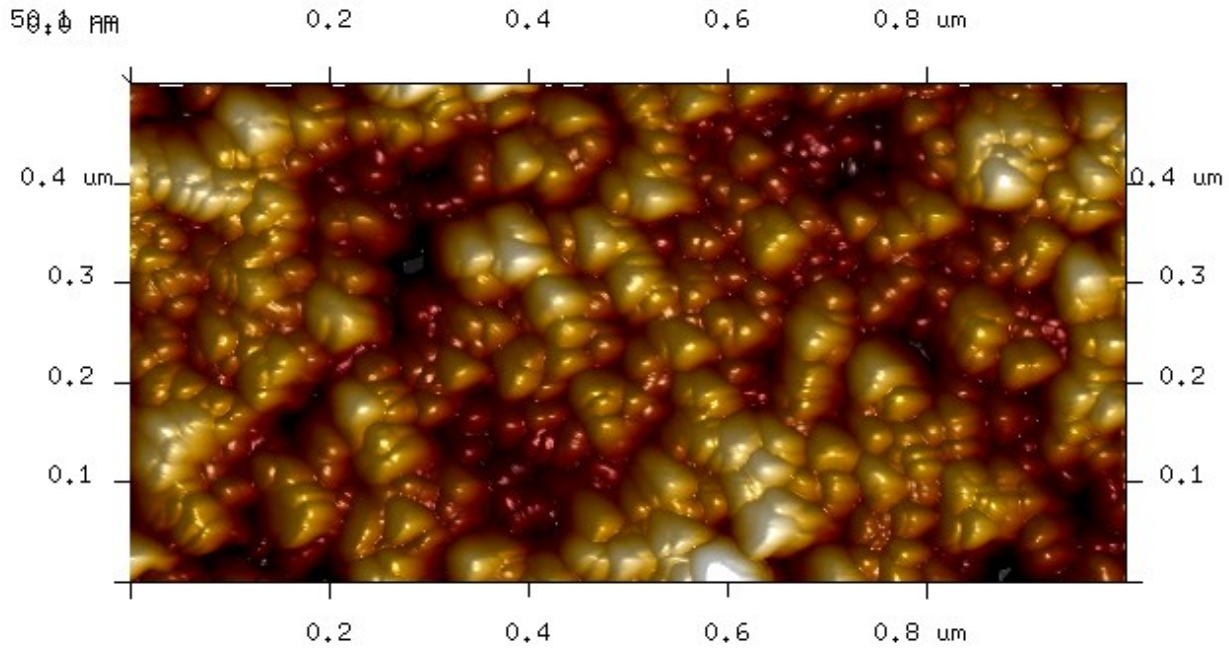

Figure S5: 3D map of the transparent TiO_2 (18NR-T) nanoparticles

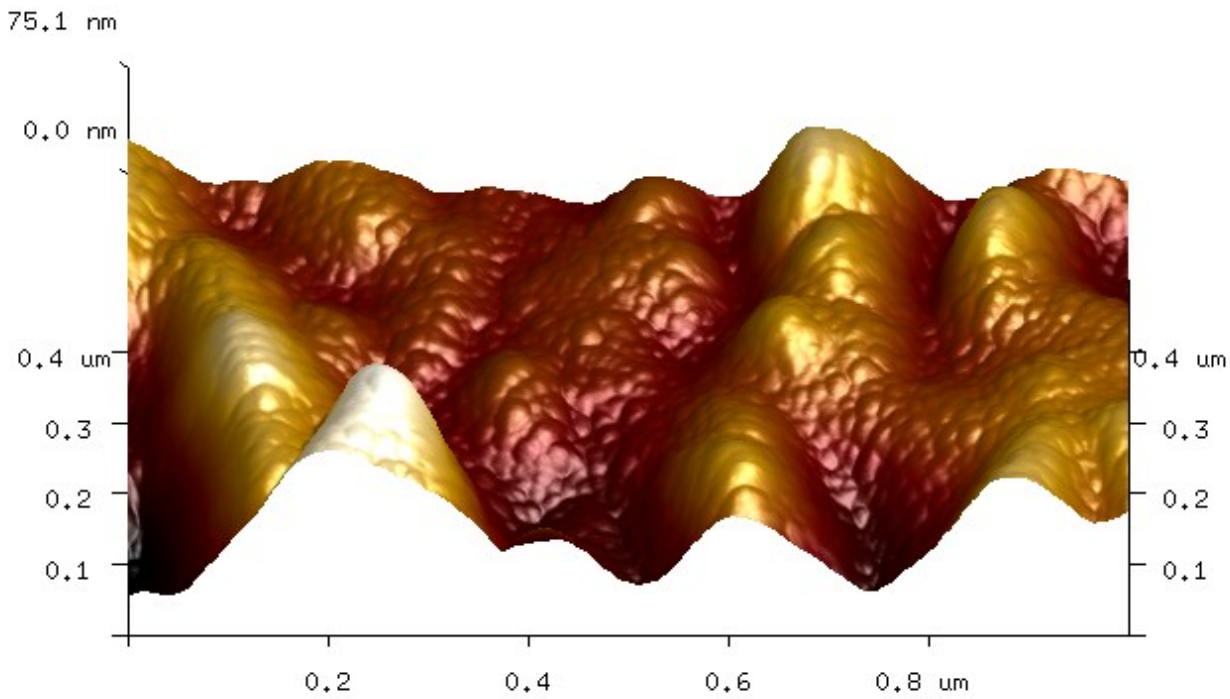

Figure S6: 3D map of FTO covered by the TiO_2 blocking underlayer (*BUL*)

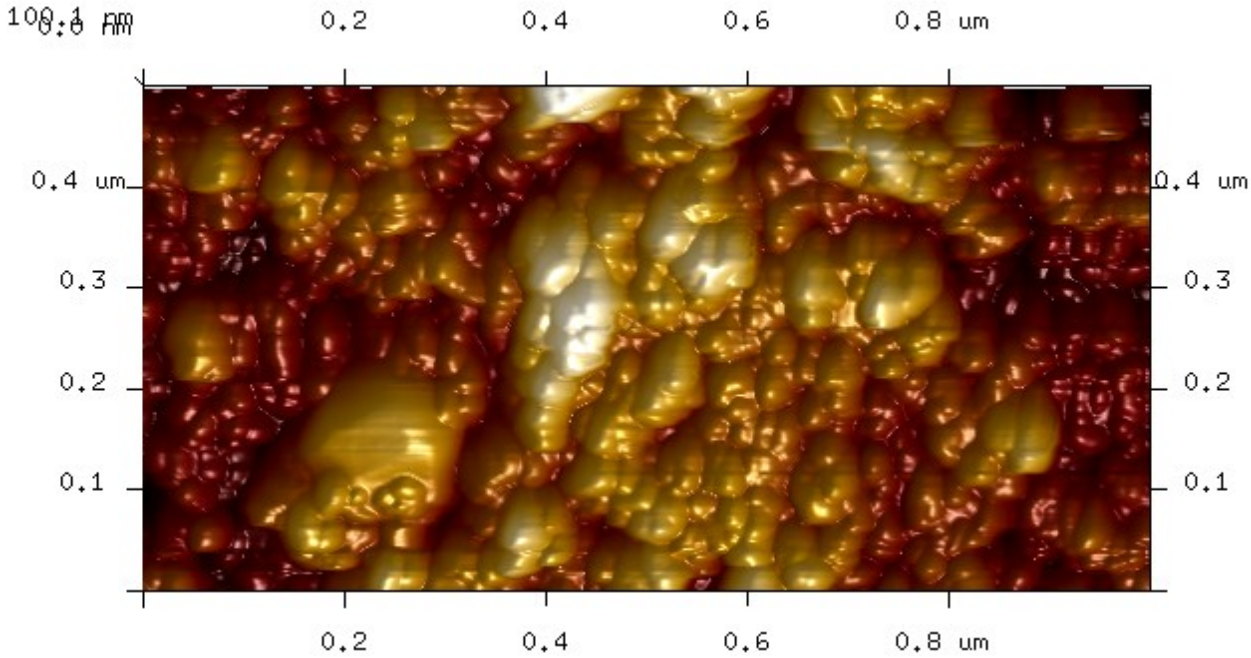

Figure S7: 3D map of the opaque TiO_2 film (18NR-AO)

7. Efficiency parameters from J/V curves

Table S1: cell efficiency parameters from **C1**/TiO_2 sensitized solar cells in the presence of different electrolytes and semiconductor substrates. As a comparison, results from N 719 sensitized solar cells assembled with *BUL-el1* are given in entry 5

Fe(II)	Voc (V)	J (mA/cm²)	FF	η %
***BUL* electrolyte 1**	0.38	3.34	59	0.75
No *BUL* electrolyte 1	0.38	2.34	55	0.49
***BUL* Opaque titania electrolyte 1**	0.42	3.55	60	0.89
***BUL* electrolyte 2**	0.44	3.30	63	0.92
N719	**Voc (V)**	**J (mA/cm²)**	**FF**	**η %**
***BUL* electrolyte 1**	0.45	12.9	53	3.09

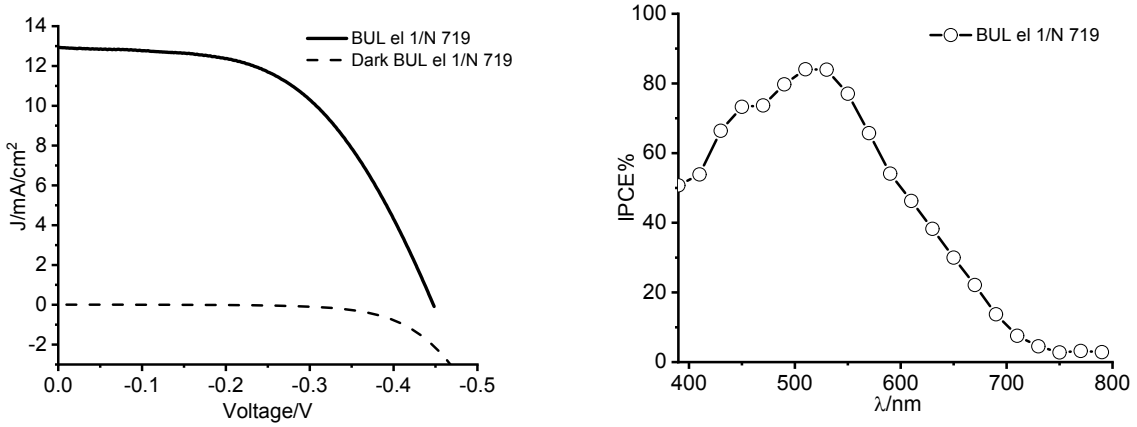

Figure S8: left: J/V curves of N 719 sensitized solar cells (*BUL-el1*) under AM 1.5G illumination in the presence of electrolyte 1; right: IPCE spectrum under short circuit

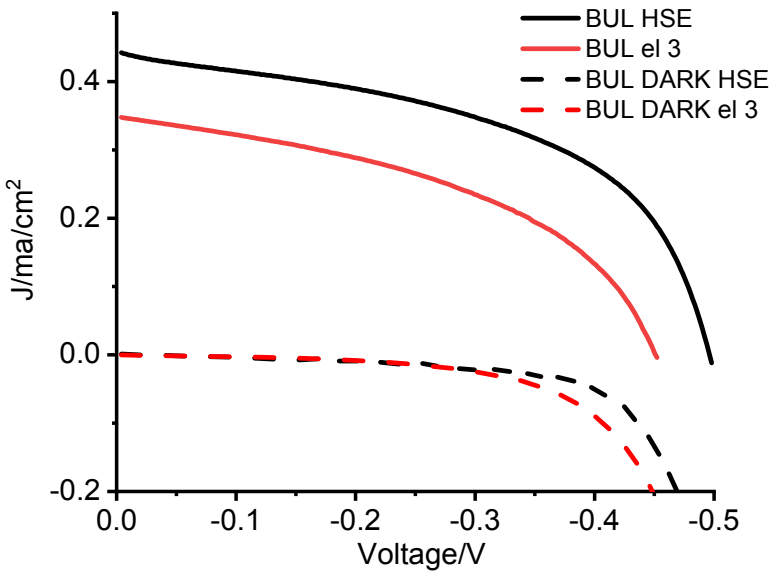

Figure S9: J/V curves of **C1**/TiO_2 sensitized solar cells under AM 1.5G illumination in the presence of HSE and 4-tBuPy

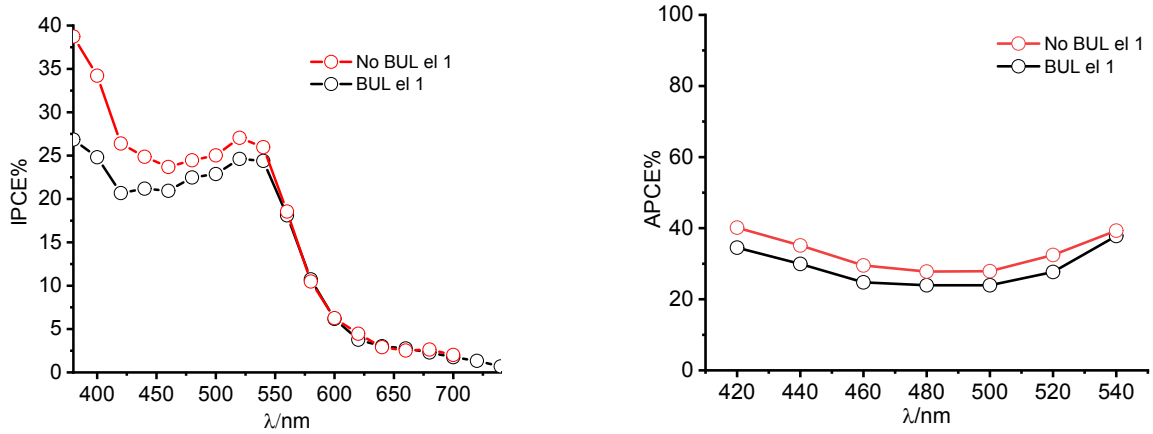

Figure S10: (left) IPCE curves recorded with transparent **C1** /SnO_2 with (black) and without (red) blocking underlayer; right: APCE spectra. Spectra recorded under + 0.2 V bias corresponding to the plateau of the J/V characteristics in Figure S11

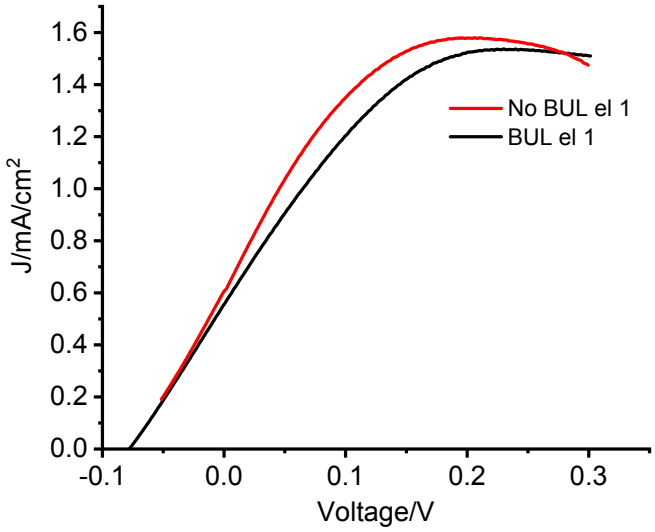

Figure S11: J/V curves of **C1** /SnO_2 sensitized solar cells under AM 1.5G illumination in the presence of *el1*

8. Transient Spectroscopy

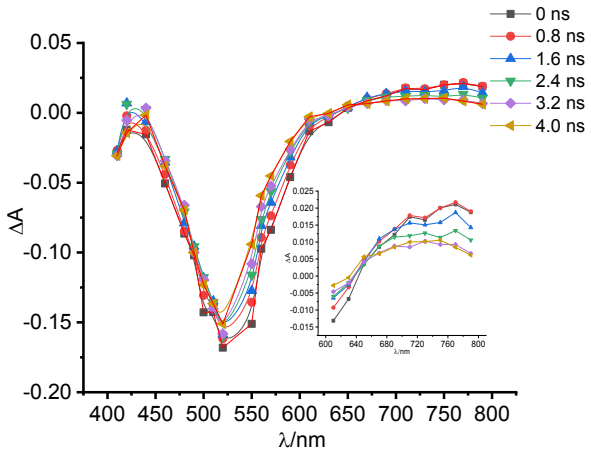

Figure S12: Spectral evolution of **C1**/TiO_2 during the first 4ns starting from the maximum of the laser pulse. Inset, magnification of the spectral region for λ> 600 nm, showing the decay of a weak absorption band which follows the same dynamics of the bleach narrowing. The sensitized film is in contact with 0.1 M $LiClO_4$ in ACN

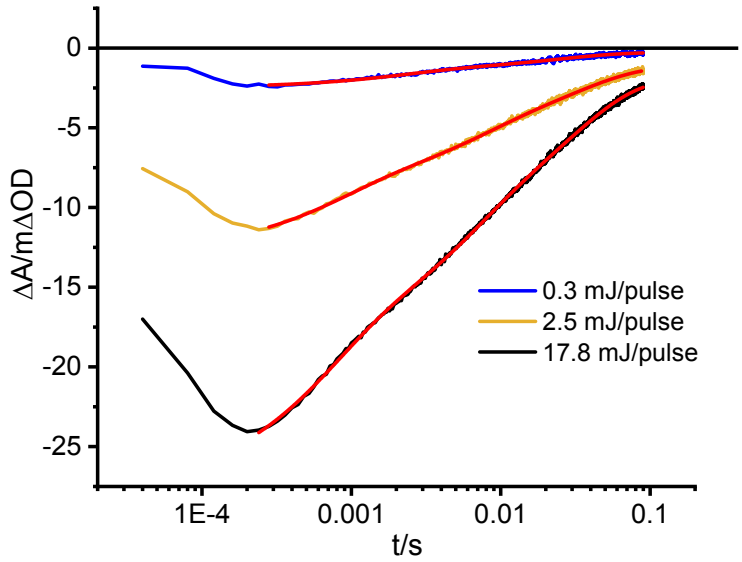

Figure S13: 500 nm charge recombination kinetics in **C1**/TiO_2 photoanodes measured under different excitation energy decreasing from 17.8 mJ/cm^2/pulse (black) to 0.3 mJ/cm^2/pulse (blue)

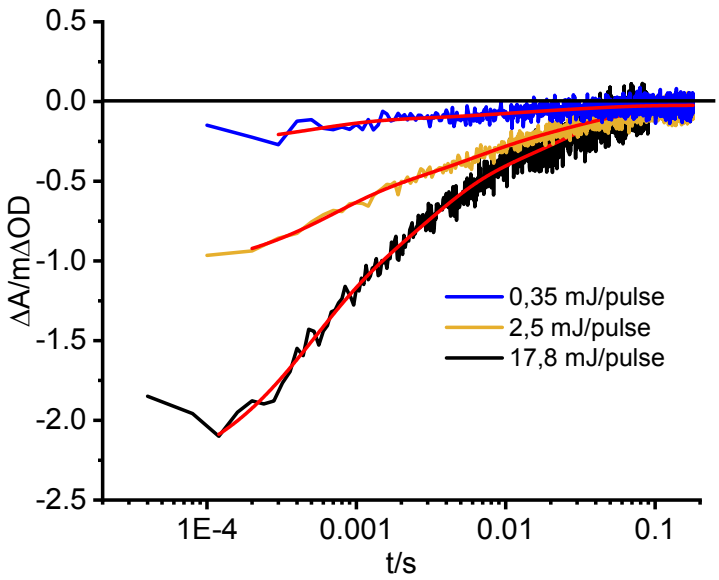

Figure S14: 500 nm charge recombination kinetics in **C1**/SnO_2 photoanodes measured under different excitation energy decreasing from 17.8 mJ/cm^2/pulse (black) to 0.35 mJ/cm^2/pulse (blue)

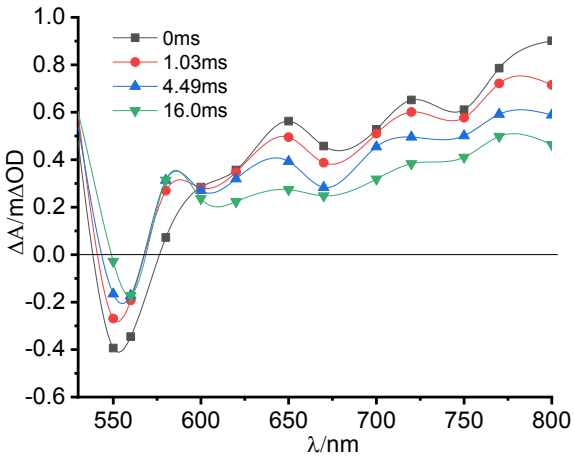

Figure S15: TA spectra for **C1**/TiO_2 in the presence of the full electrolyte 2 (containing 0.6 M PMII, 0.1 M LiI, 0.1 M GuNCS, 0.1 M MgI_2 and 0.1 M I_2)

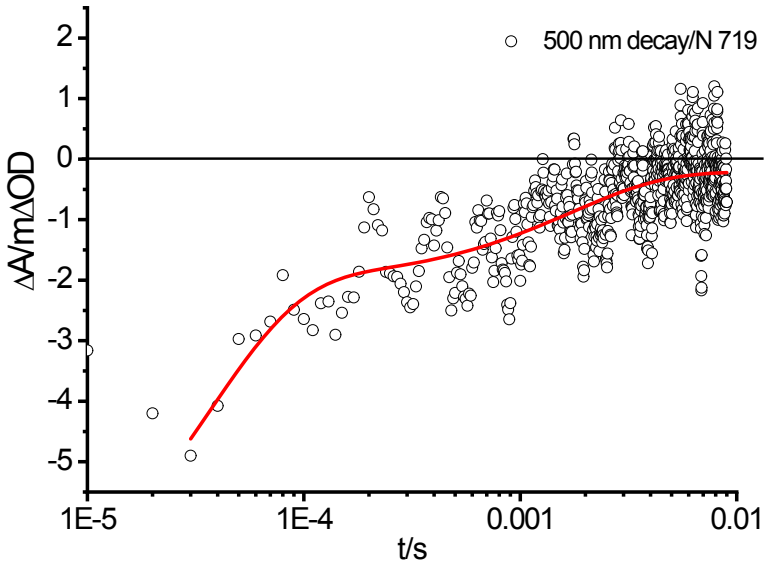

Figure S16: 500 nm charge recombination kinetics measured with N 719 loaded on TiO_2 (N719/TiO_2) in contact with 0.1 M $LiClO_4$ in ACN

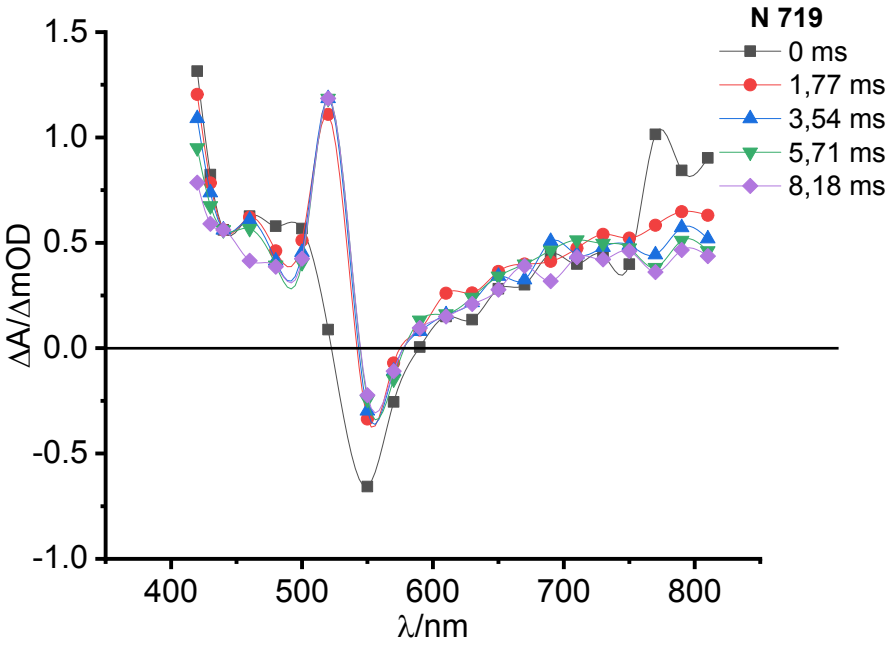

Figure S17: TA spectra in the presence of electrolyte 2 (0.6 M PMII, 0.1 M LiI, 0.1 M GuNCS, 0.1 M MgI_2 and no iodine) of N719/TiO_2. TA spectra show the sharp bleaching and the absorption due to the Stark effect and the absorption of photoinjected electrons starting from $\lambda > 600$ nm and extending into the red

9. Stark effect

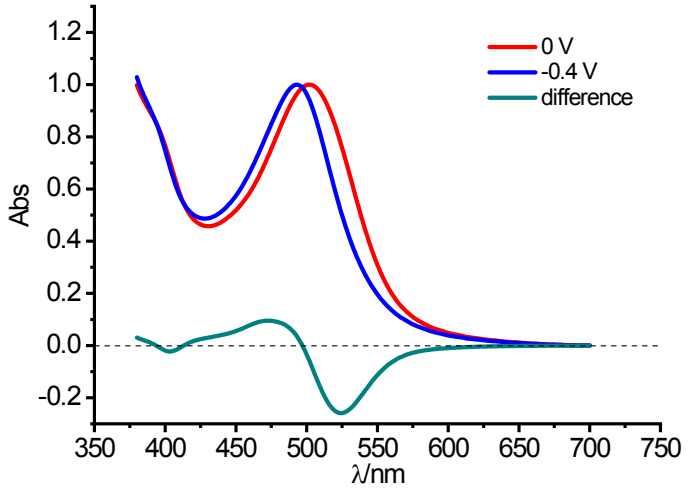

Figure S18: Absorption spectra of **C1**/TiO_2 measured in a three electrode spectroelectrochemical cell containing in 0.1M $LiClO_4$ in acetronitrile. Spectra taken at open circuit (disconnected wires) (red line) and at -0.4V vs Ag (blue line) and the resulting difference spectrum (green line) are shown

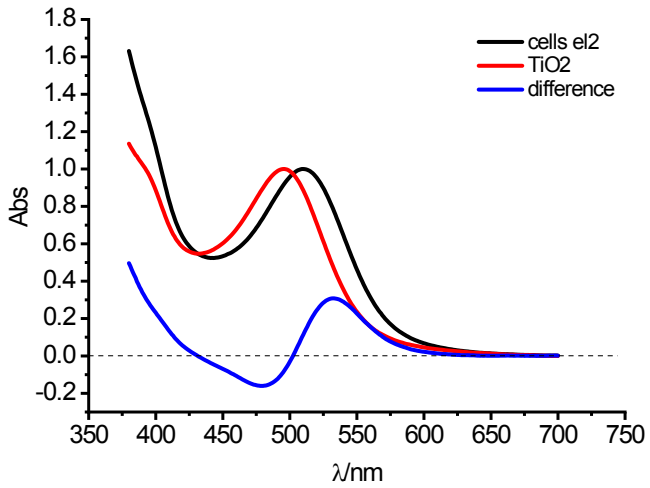

Figure S19: Absorption spectra of **C1**/TiO_2 in contact with air (red line) and in contact with the reduced form of the electrolyte 2 (0.6 M PMII, 0.1 M LiI, 0.1 M GuNCS, 0.1 M MgI_2 in ACN) (withdrawn by capillarity in an electrode sandwich configuration) (black line) and the resulting difference spectrum (blue line)

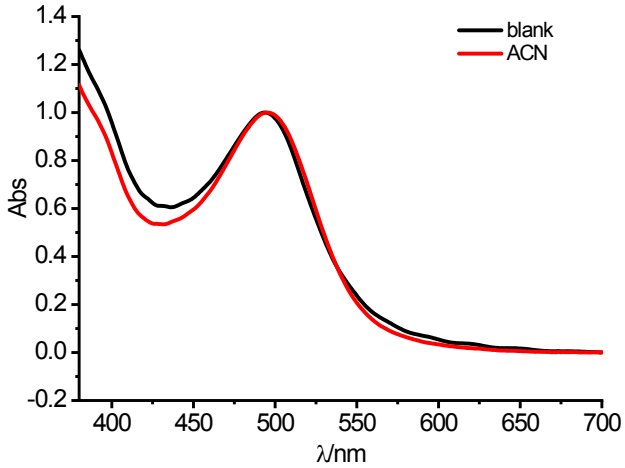

Figure S20: Absorption spectra of **C1**/TiO_2 complex with and without acetonitrile

10. Recombination of electrons with I_3^-

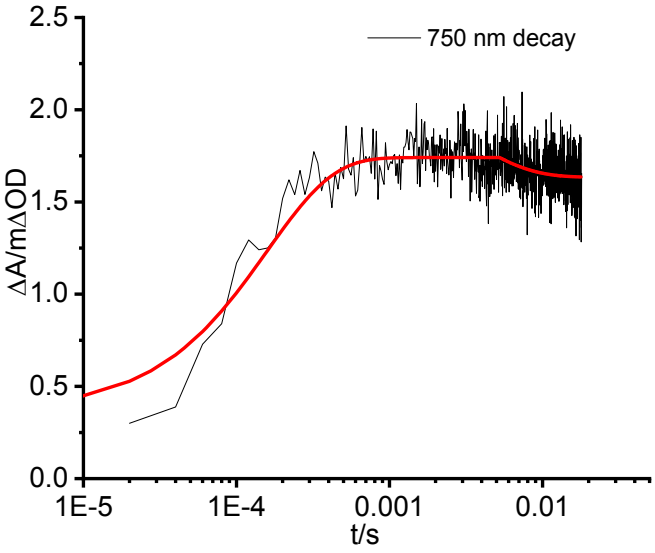

Figure S21: 750 nm electron absorption decay in **C1**/TiO_2 in the presence of the reduced form of the electrolyte 2 (0.6 M PMII, 0.1 M LiI, 0.1 M GuNCS, 0.1 M MgI_2 in ACN) without I_3^- initially present.

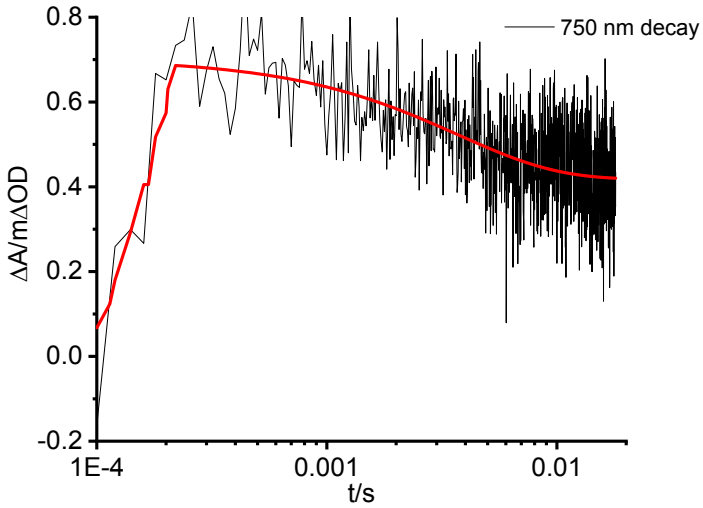

Figure S22: 750 nm electron absorption decay in **C1**/TiO_2 in the presence of the complete electrolyte 2 (0.6 M PMII, 0.1 M LiI, 0.1 M GuNCS, 0.1 M MgI_2, 0.1 M I_2 in ACN)

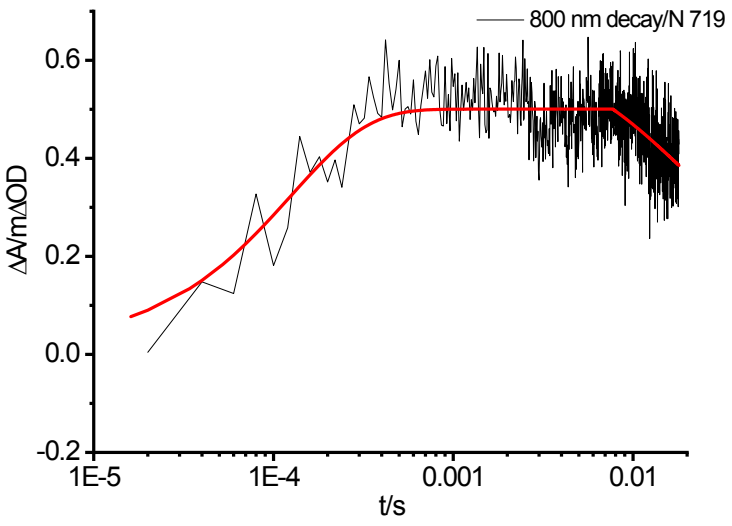

Figure S23: 800nm electron absorption decay in N 719/TiO_2 in presence of complete electrolyte 2 (0.6 M PMII, 0.1 M LiI, 0.1 M GuNCS, 0.1 M MgI_2, 0.1 M I_2 in ACN)

11. FT-IR

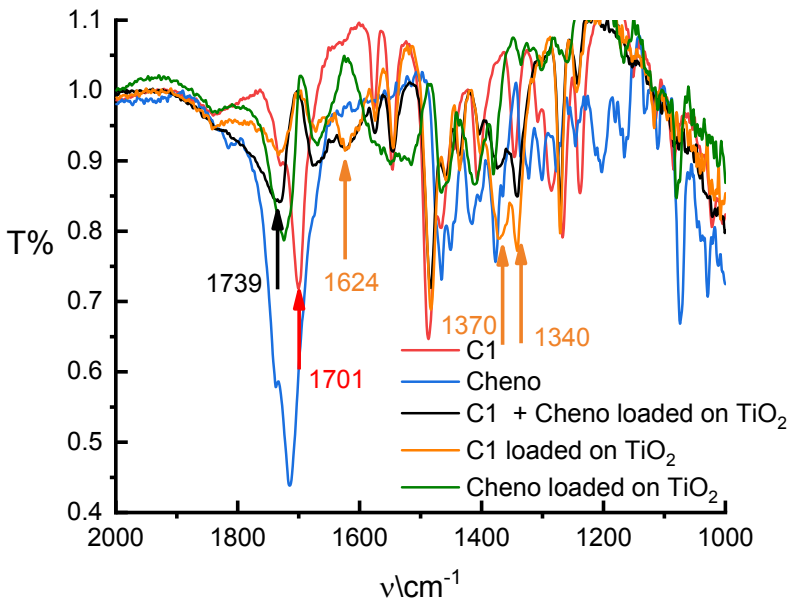

Figure S24: FT-IR spectra of **C1** loaded on TiO_2 (orange) compared to **C1** dispersed in KBr (red), **C1** loaded on TiO_2 in the presence of Chenodeoxycholic acid (black), Chenodeoxycholic acid loaded on TiO_2 (green) and Chenodeoxycholic acid dispersed in KBr matrix (blue).

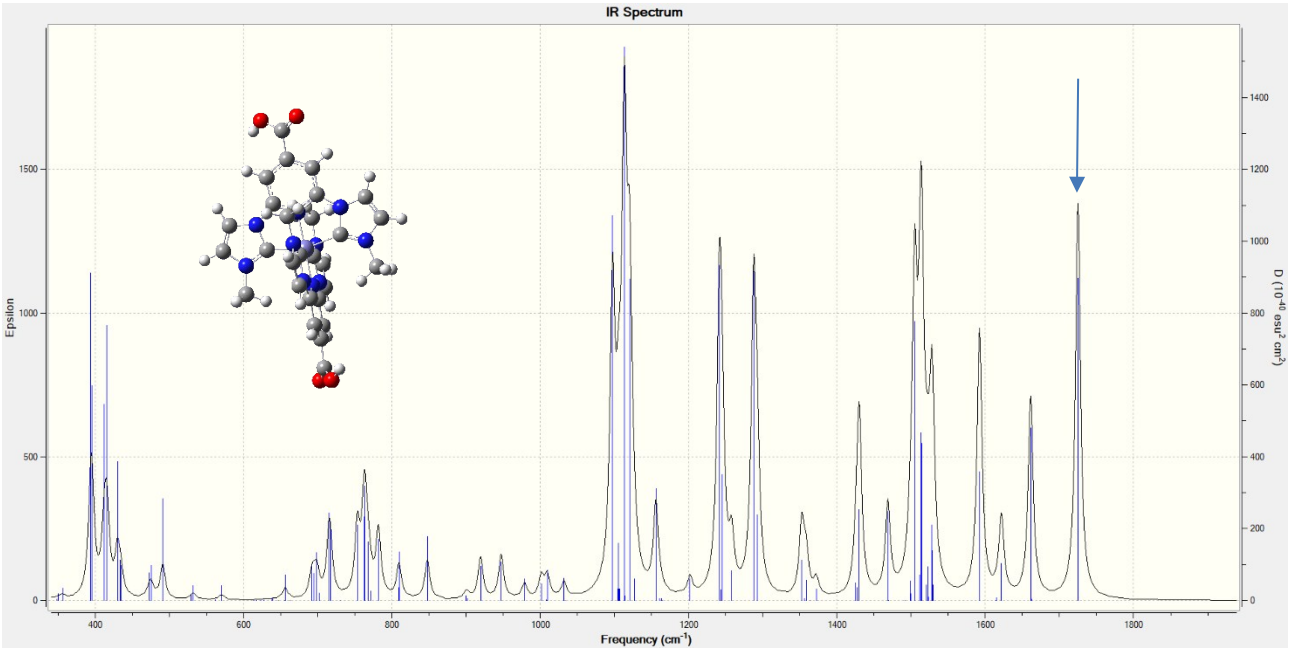

Figure S25: Computed (B3LYP-LANL2DZ) IR spectrum of **C1** in protonated form. The peak indicated by the arrow results from the asymmetric stretching of the COOH groups at 1725 cm^{-1}. Peaks at 1662 and 1621 cm^{-1} results from collective ring deformation mode involving mainly the C=C bonds.

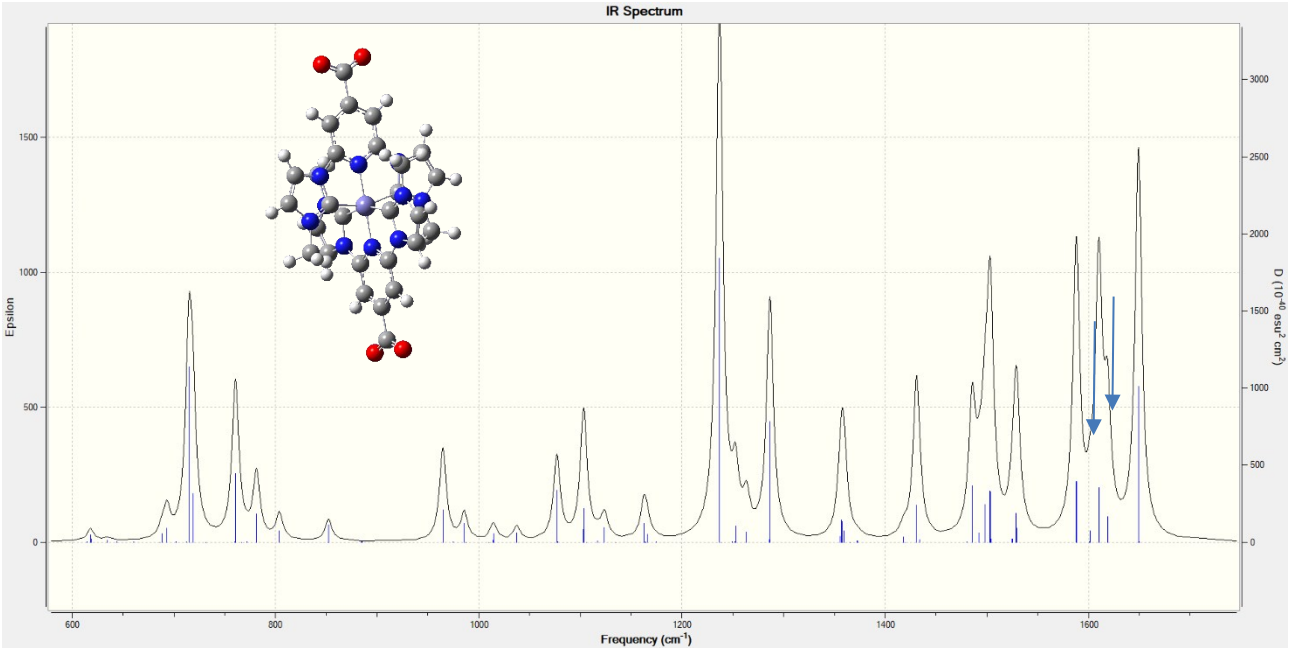

Figure S26: Computed (B3LYP-LANL2DZ) IR spectrum of **C1** in anionic form. The peaks bearing the main contribution of COO^- stretching are identified at 1610 and 1618 cm^{-1}. No IR absorption is found in the 1720 ±50 cm^{-1} region

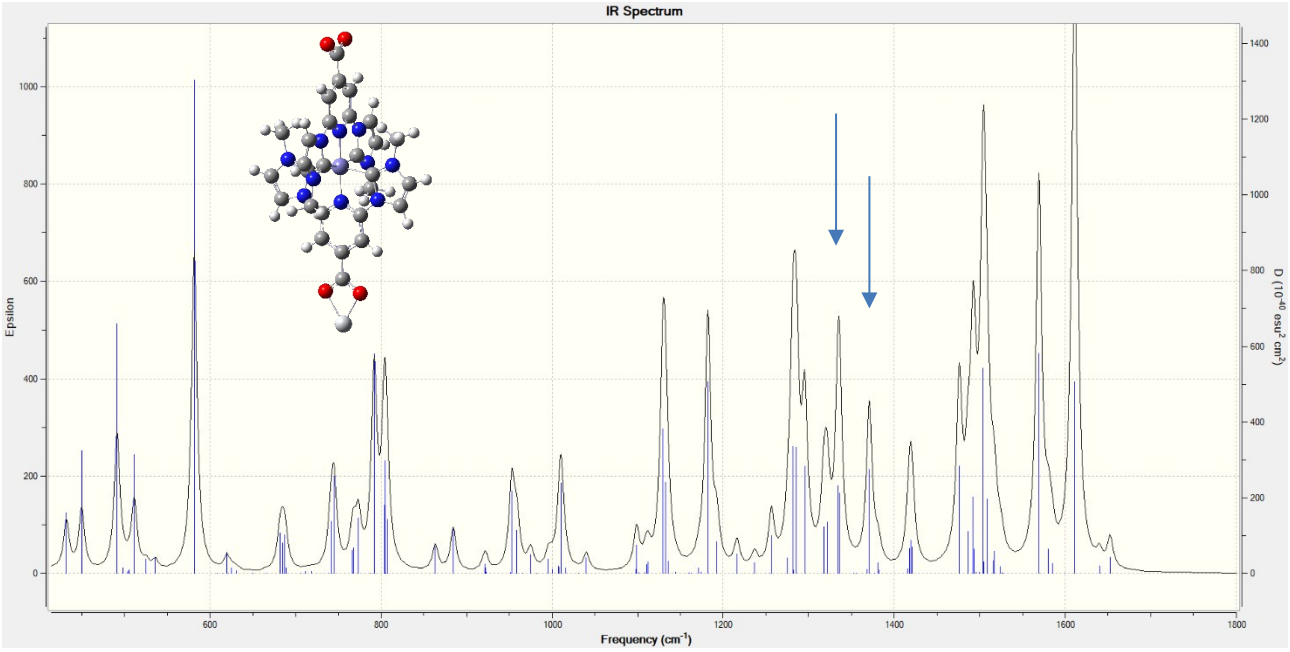

Figure S27: Computed (B3LYP-LANL2DZ) IR spectrum of **C1** in anionic form coordinated to a Ti(IV) ion. Bands indicated by arrows bear the contribution of the COO^- group coordinated to Ti(IV) and of a collective mode involving both ring deformation and asymmetric stretching of the free COO^-

The experimental IR spectra reported in Figure S24 shows the shift of the COOH stretching band of **C1** from 1701 cm^{-1} to 1739 cm^{-1}. We note that this COOH frequency is in good agreement with the computed one at 1725 cm^{-1} (blue arrow in Figure S25) in the fully protonated form. Such a shift is assigned to formation of the ester type COO-Ti bond in agreement with the literature[7]. The calculation on the fully anionic form (Figure S26) shows normal modes involving the COO^- groups at 1610 and 1618 cm^{-1}, having a relatively low intensity. These agree experimentally with the presence of a relatively broad band at 1624 cm^{-1} (Figure S24) when the dye is loaded on TiO_2, suggesting the partial formation of the fully anionic form. Chelation of COO^- to Ti(IV) also results in a band at 1336 cm^{-1}, predicted by the calculations, which is found in the experimental spectrum at 1340 cm^{-1}. When **C1** interacts with Ti(IV) another collective mode bearing the contribution of the COO^- uncoordinated to Ti(IV) is found at 1370 cm^{-1}, clearly observed when **C1** is loaded on TiO_2, but absent when the same dye is dispersed in the KBr matrix. This spectral evidence suggests that deprotonation of both carboxylic groups may occur upon interaction of the Dye with TiO_2.

References

1. R. B. Carlo Alberto Bignozzi, Eva Busatto, Stefano Caramori, Stefano Carli, Sandro Fracasso, *Patent PCT/IT2011/000397*, 2011.
2. F. Ronconi, Z. Syrgiannis, A. Bonasera, M. Prato, R. Argazzi, S. Caramori, V. Cristino and C. A. Bignozzi, *Journal of the American Chemical Society*, 2015, **137**, 4630-4633.
3. T. Duchanois, T. Etienne, C. Cebrián, L. Liu, A. Monari, M. Beley, X. Assfeld, S. Haacke and P. C. Gros, *European Journal of Inorganic Chemistry*, 2015, **2015**, 2469-2477.
4. G. Di Carlo, S. Caramori, L. Casarin, A. Orbelli Biroli, F. Tessore, R. Argazzi, A. Oriana, G. Cerullo, C. A. Bignozzi and M. Pizzotti, *The Journal of Physical Chemistry C*, 2017, **121**, 18385-18400.
5. S. Carli, L. Casarin, G. Bergamini, S. Caramori and C. A. Bignozzi, *The Journal of Physical Chemistry C*, 2014, **118**, 16782-16790.
6. M. Adachi, M. Sakamoto, J. Jiu, Y. Ogata and S. Isoda, *The Journal of Physical Chemistry B*, 2006, **110**, 13872-13880.
7. R. Argazzi, C. A. Bignozzi, T. A. Heimer, F. N. Castellano and G. J. Meyer, *Inorganic Chemistry*, 1994, **33**, 5741-5749.